Chance Constrained Reserve Scheduling Using Uncertain Controllable Loads Part II: Analytical Reformulation

Bowen Li, *Student Member, IEEE*, Maria Vrakopoulou, *Member, IEEE*, and Johanna L. Mathieu, *Member, IEEE*

***Abstract*—This paper is Part II of a two-part paper that develops a multi-period chance constrained optimal power flow model to schedule generation and reserves from both generators and aggregations of uncertain but controllable electric loads. Part I developed the formulation and solved the problem using a scenario-based method. In Part II, we assume that all uncertainties follow multivariate normal distributions, allowing us to reformulate the constraints analytically to obtain a deterministic formulation that can be solved faster and with less need for real data than the scenario-based method in Part I. We test the approach on a modified IEEE 30-bus system and compare the solutions, empirical reliabilities, and computational requirements to those of the scenario-based method. We find that the analytical reformulation solved using a cutting plane algorithm requires less computational time than the scenario-based method. Additionally, its solution is less costly and less conservative; however, its empirical reliability is lower, though still close to the desired reliability.**

***Index Terms*—Chance constrained optimization, load control, multi-period optimal power flow, normally-distributed uncertainty, wind power integration.**

I. Introduction

In PART I of this two part paper, we formulated a multi-period chance-constrained optimal power flow (CC-OPF) problem to schedule generator production and load consumption set points along with both generator and load-based reserve capacities assuming wind power and outdoor temperature forecast uncertainty. The latter affects the available reserve capacities from controllable loads, which are assumed to be residential thermostatically controlled loads. We solved the problem using a scenario-based method [1] that results in a probabilistically robust reformulation of the CC-OPF problem. We showed that the method's reliability guarantees are satisfied empirically, but that the solution may be conservative with reliability levels far of excess of required reliability levels.

Manuscript received March 19, 2017; revised July 5, 2017 and September 27, 2017; accepted November 9, 2017. Date of publication November 15, 2017; date of current version February 18, 2019. This work was supported in part by the U.S. NSF under Grant CCF-1442495, and in part by the European Commission through the Project SOPRIS under Grant PIOF-GA-2013-626014. Paper no. TSG-00385-2017. *(Corresponding author: Johanna L. Mathieu.)*

B. Li and J. L. Mathieu are with the Department of Electrical Engineering and Computer Science, University of Michigan, Ann Arbor, MI 48109 USA (e-mail: libowen@umich.edu; jlmath@umich.edu).

M. Vrakopoulou is with the Automatic Control Laboratory, ETH Zurich, 8092 Zurich, Switzerland (e-mail: vrakopoulou@control.ee.ethz.ch).

Digital Object Identifier 10.1109/TSG.2017.2773603

In Part II, we analytically reformulate the problem assuming that wind and outdoor temperature forecast uncertainty follow multivariate normal distributions. In reality, the errors may not follow these distributions; however, the assumption allows us to solve the problem faster and with less need for real data (i.e., uncertainty scenarios), at the cost of less reliable solutions. References [2], [3] also analytically reformulate CC-OPF problems, but they do not consider controllable loads. Reference [4] analytically reformulates a *single-period* CC-OPF problem with uncertain controllable loads, whereas we reformulate the *multi-period problem*, a much more complex task. Moreover, [4] assumed load power/energy capacity and baseline uncertainty were each normally distributed and uncorrelated, whereas we assume only the underlying uncertainty, i.e., temperature forecast error, is normally distributed. The latter is a much more realistic assumption; however, it makes the problem much more difficult to solve. In particular, using a piecewise linear model for the load power and energy capacities, the probabilistic upper power/energy capacity constraints are joint chance constraints that can not be reformulated analytically. Instead we derive confidence bounds and show through empirical examples and a proof sketch that they are convex.

The reformulated problem is a deterministic, nonlinear optimization problem, which we show to be convex. We solve the problem in two ways: using a nonlinear solver and using an iterative cutting plane approach [2] that introduces linear approximations of the nonlinear constraints only when they are binding. We compare the solutions, empirical reliabilities, and computational requirements of both solving methods to those of the scenario-based method presented in Part I. To assess solution reliability, we use the realistic (i.e., non-normally distributed) uncertainty scenarios used in Part I.

Part II is organized as follows. Section II gives our assumptions, notation, and approximations. Section III derives the reformulation and describes the cutting plane algorithm. Section IV presents the case studies and Section V provides concluding remarks. Supporting analysis and proofs are provided in the Appendices.

II. Assumptions, Notation, and Approximations

Since asymmetric reserve deployment policies may result in a non-convex analytical reformulation, we assume symmetric

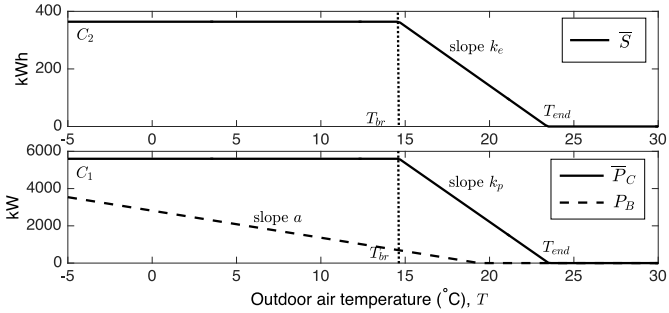

Fig. 1. Approximate energy capacity, power capacity, and baseline power consumption of an aggregation of electric heaters.

reserve deployment policies, i.e., $\overline{d} = \underline{d}$. We assume wind power forecast error and temperature forecast error follow multivariate normal distributions, where wind power forecast errors are correlated and temperature forecast errors are correlated, but wind power and temperature forecast errors are independent.

A. Notation

Unless otherwise stated, we use the same notation as in Part I and refer to Part I equations using equation references (PI-#). New uncertainty notation is defined in this section. The wind power forecast error vector is denoted $\Delta P_{W,t} \in \mathbb{R}^{N_W}$, with $\mu_{W,t} \in \mathbb{R}^{N_W}$ as its mean, $\Sigma_{W,t} \in \mathbb{R}^{N_W \times N_W}$ as its covariance, and $\delta_{W,t} \in \mathbb{R}^{N_W}$ as its standard deviation. The mean and standard deviation of the total wind power forecast error $P_{m,t} = \mathbf{1}^T \Delta P_{W,t} \in \mathbb{R}$ are denoted $\overline{\mu}_{W,t} \in \mathbb{R}$ and $\overline{\delta}_{W,t} \in \mathbb{R}$, respectively. The vector of temperature forecast errors corresponding to each controllable load aggregation is denoted $\Delta T_t \in \mathbb{R}^{N_C}$, where N_C is the number of controllable load aggregations. Recall from Part I that $\Delta P_{B,t} \in \mathbb{R}^{N_C}$ is the baseline power forecast error. Let $\mu_{B,t} \in \mathbb{R}^{N_C}$ be its mean, $\Sigma_{B,t} \in \mathbb{R}^{N_C \times N_C}$ be its covariance, and $\delta_{B,t} \in \mathbb{R}^{N_C}$ be its standard deviation. The mean and standard deviation of the total baseline power forecast error $P^b_{m,t} = \mathbf{1}^T \Delta P_{B,t} \in \mathbb{R}$ are denoted $\overline{\mu}_{B,t} \in \mathbb{R}$ and $\overline{\delta}_{B,t} \in \mathbb{R}$, respectively.

To simplify the equations that follow, vector operators (e.g., $\max(u)$, $\min(u)$, uv, u^2, $\sqrt{u}$, where u and v are arbitrary vectors) are applied element-wise.

B. Approximate Controllable Load Capacities and Baseline

To facilitate the analytical reformulation, we approximate the relationships shown in Fig. 1 of Part I. Specifically, we assume $\overline{P}_C$ and $\overline{S}$ are piecewise linear in T_t, and $\Delta P_{B,t}$ is linear in ΔT_t:

$$\overline{P}_C(T_t) = C_1 + \min\big(0, k_p(T_t - T_{br})\big), \tag{1}$$

$$\overline{S}(T_t) = C_2 + \min(0, k_e(T_t - T_{br})), \tag{2}$$

$$\Delta P_{B,t} = a \Delta T_t, \tag{3}$$

where the slopes k_p, k_e, and a; intercepts C_1 and C_2; and "breaking temperature" T_{br} are shown in Fig. 1. The slopes k_p and k_e are computed using linear regression on the data between T_{br} and the "ending temperature" T_{end}, and a is computed using linear regression on the data within the temperature forecast range. We do not approximate the relationship between the baseline power and temperature forecast $P_B(T_t^f)$ but use Fig. 1 of Part I as a look-up table, as in Part I.

III. Analytical Reformulation

In this section, we analytically reformulate (PI-38)–(PI-47). A key difference between the formulation of Part I and the analytical reformulation is that the former satisfies chance constraints *jointly*, i.e., all constraints within an hour are satisfied with probability $1 - \varepsilon$, while the latter satisfies chance constraints *individually*, i.e., each constraint is satisfied with probability $1-\varepsilon$. While the resulting formulations are different, their solutions can be compared by computing their empirical joint and individual reliabilities, which we do in Section IV.

A. General Reformulation

Assume that a random vector ξ follows a multivariate normal distribution with mean μ and covariance Σ. Then the following constraints are equivalent [5]:

$$\mathbb{P}\big(a(x)^T \xi + b(x) \le 0\big) \ge 1 - \varepsilon, \tag{4}$$

$$a(x)^T \mu + b(x) + c\sqrt{a(x)^T \Sigma a(x)} \le 0, \tag{5}$$

where $a(x)$ and $b(x)$ are functions of the decision variable x, and $c = \Phi_N^{-1}(1 - \varepsilon)$, where Φ_N denotes the cumulative distribution function (CDF) of the standard normal distribution. When $a(x)$ and $b(x)$ are affine functions of x and $\varepsilon \le 0.5$, the reformulation (5) is convex.

Constraint (5) can also be written as

$$a(x)^T \mu + b(x) + \mathcal{S} \le 0, \tag{6}$$

$$\mathcal{S} \ge c\sqrt{a(x)^T \Sigma a(x)}, \tag{7}$$

where $\mathcal{S}$ is a slack variable and (7) is a second order cone (SOC) constraint. We will reformulate the constraints into this form since it will allow us to apply a computationally-efficient cutting plane algorithm, described in Section III-D.

B. Specific Reformulation

1) Generation Constraints: Constraints (PI-39) for *Operating Point 1* are reformulated as

$$P_{G,t} - d_{GS,t}\overline{\mu}_{W,t} + d^b_{GD,t}\overline{\mu}_{B,t} + \mathcal{S}_{GS,t} \le \overline{P}_G, \tag{8}$$

$$P_{G,t} - d_{GS,t}\overline{\mu}_{W,t} + d^b_{GD,t}\overline{\mu}_{B,t} - \mathcal{S}_{GS,t} \ge \underline{P}_G, \tag{9}$$

$$\mathcal{S}_{GS,t} \ge c\sqrt{\big(d_{GS,t}\overline{\delta}_{W,t}\big)^2 + \Big(d^b_{GD,t}\overline{\delta}_{B,t}\Big)^2}, \tag{10}$$

where $\mathcal{S}_{GS,t}$ is a slack variable. Constraints (PI-39) for *Operating Points 2* and 3 can be reformulated similarly.

2) Controllable Load Power Capacity Constraints: The lower constraint of (PI-40) for *Operating Point 1* is reformulated as

$$P_{C,t} + d_{LS,t}\overline{\mu}_{W,t} + \mu_{B,t} - \mathcal{S}_{LS,t} \ge 0, \tag{11}$$

$$\mathcal{S}_{LS,t} \ge c\sqrt{\big(d_{LS,t}\overline{\delta}_{W,t}\big)^2 + \big(\delta_{B,t}\big)^2}, \tag{12}$$

where $\mathcal{S}_{LS,t}$ is a slack variable. The lower constraints of (PI-40) for *Operating Points 2* and 3 can be reformulated similarly.

The upper constraint of (PI-40) is more difficult to reformulate. Recall that the upper constraint for (PI-40) for *Operating Point 1* is

$$P_{C,t} + R_{LS,t} + R^b_{LD,t} \le \overline{P}_C(T_t), \tag{13}$$

which can be rewritten as

$$P_{C,t} + Z \le \overline{P}_C(T^f_t), \tag{14}$$

where Z contains the random variables, i.e., $Z = R_{LS,t} + \Delta P_{B,t} - e_{\overline{P}_C,t}$, where $e_{\overline{P}_C,t} = \overline{P}_C(T_t) - \overline{P}_C(T^f_t)$. We can rewrite Z in terms of $P_{m,t}$ and ΔT_t, by considering two cases.

a) Case 1, $T^f_t < T_{br}$: Referring to Fig. 1, denote the positive difference between the forecast and the breaking temperature as $e_{T,t} = T_{br} - T^f_t$. Then, $e_{\overline{P}_C,t} = \min(0, k_p(\Delta T_t - e_{T,t}))$ and $Z = d_{LS,t}P_{m,t} + \max(a\Delta T_t, (a-k_p)\Delta T_t + k_p e_{T,t})$.

b) Case 2, $T_{br} < T^f_t < T_{end}$: Referring to Fig. 1, $e_{\overline{P}_C,t} = \min(C_1 - \overline{P}_c(T^f_t), k_p\Delta T_t)$ and $Z = d_{LS,t}P_{m,t} + \max(a\Delta T_t + \overline{P}_c(T^f_t) - C_1, (a-k_p)\Delta T_t)$.

Both expressions for Z and the corresponding expressions for *Operating Point 2* are of the form

$$Z = \max(k_1 X, k_2 X + h) + dY = M + dY, \tag{15}$$

where $X = \Delta T_t$, $Y = P_{m,t}$, $d = d_{LS,t}$, and k_1, k_2, and h are constants. In each case, (14) is a joint chance constraint, for example, for *Operating Point 1*, case 1 (14) is

$$\mathbb{P}\begin{pmatrix} P_{C,t} + d_{LS,t}P_{m,t} + a\Delta T_t \le \overline{P}_C(T^f_t) \\ P_{C,t} + d_{LS,t}P_{m,t} + (a-k_p)\Delta T_t + \\ \qquad k_p e_{T,t} \le \overline{P}_C(T^f_t) \end{pmatrix} \ge 1 - \epsilon \tag{16}$$

Ongoing research is seeking methods to reformulate joint chance constraints; however, existing approaches, e.g., [6] can only be applied to constraints with specific forms. Unfortunately, we are unaware of any approaches that can be used to reformulate constraints of the form of (16). Therefore, in Appendix A, we develop a technique to empirically compute a confidence bound z_1 for Z, such that $\mathbb{P}(Z \le z_1(d_{LS,t})) \ge 1 - \varepsilon$, which allows us to reformulate the upper constraint of (PI-40) as

$$P_{C,t} + z_1(d_{LS,t}) \le \overline{P}_C\Big(T^f_t\Big), \tag{17}$$

which is nonlinear but convex as shown in Appendix B.

Unfortunately, the corresponding expressions for *Operating Point 3* are not of the form (15), specifically, $Z = R_{LS,t} + R^{w0}_{LD,t} + R^{b0}_{LD,t} - e_{\overline{P}_C,t} = d_{LS,t}P_{m,t} - d_{LS,t-1}P_{m,t-1} + a\Delta T_{t-1} - e_{\overline{P}_C,t}(\Delta T_t)$, which includes four random variables. While it would be possible to analytically reformulate the corresponding constraint, we instead approximate it as

$$P_{C,t} + d_{LS,t}\widetilde{P}_{m,t} + R^{w0}_{LD,t} + R^{b0}_{LD,t} \le \overline{P}_C\Big(T^f_t + \Delta\widetilde{T}_t\Big), \tag{18}$$

where we have replaced $P_{m,t}$ with $\widetilde{P}_{m,t}$, ΔT_t with $\Delta\widetilde{T}_t$, and used the definition of $e_{\overline{P}_C,t}$. The approximate $\widetilde{P}_{m,t}$ uses the wind power forecast error statistics from $t-1$ rather than t and $\Delta\widetilde{T}_t = \Delta T_{t-1}$. The approximate constraint can be reformulated as (17), where its confidence bound can be computed using the method described in Appendix A. The approximation is physically justified because wind power forecast statistics and temperature forecast errors should be similar between hours. We demonstrate the impact of the approximation through case studies in Section IV.

3) Reserve Capacity Constraints: Constraints (PI-41) – (PI-43) are reformulated as

$$\overline{R}_{GS,t} \ge -d_{GS,t}\overline{\mu}_{W,t} + cd_{GS,t}\overline{\delta}_{W,t}, \tag{19}$$

$$\underline{R}_{GS,t} \ge d_{GS,t}\overline{\mu}_{W,t} + cd_{GS,t}\overline{\delta}_{W,t}, \tag{20}$$

$$\overline{R}_{LS,t} \ge d_{LS,t}\overline{\mu}_{W,t} + cd_{LS,t}\overline{\delta}_{W,t}, \tag{21}$$

$$\underline{R}_{LS,t} \ge -d_{LS,t}\overline{\mu}_{W,t} + cd_{LS,t}\overline{\delta}_{W,t}, \tag{22}$$

$$\overline{R}_{GD,t} \ge d^b_{GD,t}\overline{\mu}_{B,t} + cd^b_{GD,t}\overline{\delta}_{B,t}, \tag{23}$$

$$\underline{R}_{GD,t} \ge -d^b_{GD,t}\overline{\mu}_{B,t} + cd^b_{GS,t}\overline{\delta}_{B,t}. \tag{24}$$

Constraints (PI-44) and (PI-45) can be reformulated similarly.

4) Controllable Load Energy Capacity Constraints: The lower constraints of (PI-46) and (PI-47) are reformulated as

$$S_t + \Big(P_{C,t} - P_B\Big(T^f_t\Big) + d_{LS,t}\overline{\mu}_{W,t} - \mu_{B,t}\Big)\frac{\Delta\tau}{n} - \mathcal{S}_{EC,t} \ge 0, \tag{25}$$

$$S_t + \Big(P_{C,t} - P_B\Big(T^f_t\Big)\Big)\Delta\tau + \big(d_{LS,t}\overline{\mu}_{W,t} - \mu_{B,t}\big)\frac{\Delta\tau}{n} - \mathcal{S}_{EC,t} \ge 0, \tag{26}$$

$$\mathcal{S}_{EC,t} \ge \frac{c\Delta\tau}{n}\sqrt{\big(d_{LS,t}\overline{\delta}_{W,t}\big)^2 + \big(\delta_{B,t}\big)^2}, \tag{27}$$

where $\mathcal{S}_{EC,t}$ is a slack variable.

Like the upper power capacity constraints, the upper energy capacity constraints are more difficult to reformulate. The portion of the constraints that contains the random variables is $Z = (R_{LS,t} - \Delta P_{B,t})\Delta\tau/n - e_{\overline{S},t}$, where $e_{\overline{S},t} = \overline{S}(T_t) - \overline{S}(T^f_t)$. As before, we can rewrite Z in terms of $P_{m,t}$ and ΔT_t, by considering two cases.

a) Case 1, $T^f_t < T_{br}$: Referring to Fig. 1, $e_{\overline{S},t} = \min(0, k_e(\Delta T_t - e_{T,t}))$ and

$$Z = d_{LS,t}P_{m,t}\frac{\Delta\tau}{n} + \max\Big(-a\Delta T_t\frac{\Delta\tau}{n} - k_e\big(\Delta T_t - e_{T,t}\big), - a\Delta T_t\frac{\Delta\tau}{n}\Big).$$

b) Case 2, $T_{br} < T^f_t < T_{end}$: Referring to Fig. 1, $e_{\overline{S},t} = \min(C_2 - \overline{S}(T^f_t), k_e\Delta T_t)$ and

$$Z = d_{LS,t}P_{m,t}\frac{\Delta\tau}{n} + \max\Big(-a\Delta T_t\frac{\Delta\tau}{n} - C_2 + \overline{S}\Big(T^f_t\Big), - a\Delta T_t\frac{\Delta\tau}{n} - k_e\Delta T_t\Big).$$

Again, both expressions for Z are of the form (15) (though now Y is a fraction of $P_{m,t}$) and so we can reformulate the constraints as

$$S_t + \Big(P_{C,t} - P_B(T^f_t)\Big)\frac{\Delta\tau}{n} + z_2(d_{LS,t}) \le \overline{S}\Big(T^f_t\Big), \tag{28}$$

$$S_t + \Big(P_{C,t} - P_B\Big(T^f_t\Big)\Big)\Delta\tau + z_2(d_{LS,t}) \le \overline{S}\Big(T^f_t\Big), \tag{29}$$

where z_2 is the confidence bound computed using the method described in Appendix A. These constraints are nonlinear but convex as shown in Appendix B.

5) Power Flow Constraints: Constraints (PI-38) include all wind power and temperature forecast errors. First, we express (PI-37) as $P^{new}_{inj,t} = P^{f}_{inj,t} + P^{w}_{inj,t} + P^{b}_{inj,t}$ where, for *Operating Point 1*,

$$P^{f}_{inj,t} = C_G P_{G,t} + C_W P^{f}_{W,t} - C_L\big(P_{L,t} + P_{C,t}\big), \tag{30}$$

$$P^{w}_{inj,t} = -C_G d_{GS,t} P_{m,t} + C_W \Delta P_{W,t} - C_L d_{LS,t} P_{m,t}, \tag{31}$$

$$P^{b}_{inj,t} = C_G d^{b}_{GD,t} P^{b}_{m,t} - C_L \Delta P_{B,t}. \tag{32}$$

Next, we define the power flows $P_t = AP^{new}_{inj,t} = P^{f}_{t} + P^{w}_{t} + P^{b}_{t}$ where, for *Operating Point 1*,

$$P^{f}_{t} = A_G P_{G,t} + A_W P^{f}_{W,t} - A_L\big(P_{L,t} + P_{C,t}\big), \tag{33}$$

$$P^{w}_{t} = D_{W,t}\big(d_{GS,t}, d_{LS,t}\big)\Delta P_{W,t}, \tag{34}$$

$$P^{b}_{t} = D_{B,t}\Big(d^{b}_{GD,t}\Big)\Delta P_{B,t}, \tag{35}$$

where $A_G = AC_G, A_W = AC_W$, and $A_L = AC_L$. The matrices $D_{W,t}$ and $D_{B,t}$ include A_G, A_W, A_L, and the distribution vectors as linear functions of the random variables.

Let subscript i refer to the i^{th} row of a vector/matrix. The power flow constraints for each line i for *Operating Point 1* are

$$P^{f}_{t,i} + D_{W,t,i}\mu_{W,t} + D_{B,t,i}\mu_{B,t} + \mathcal{S}_{L,t,i} \le P_{l,i}, \tag{36}$$

$$P^{f}_{t,i} + D_{W,t,i}\mu_{W,t} + D_{B,t,i}\mu_{B,t} - \mathcal{S}_{L,t,i} \ge -P_{l,i}, \tag{37}$$

$$\mathcal{S}_{L,t,i} \ge c\sqrt{D^{T}_{W,t,i}\Sigma_{W,t}D_{W,t,i} + D^{T}_{B,t,i}\Sigma_{B,t}D_{B,t,i}}, \tag{38}$$

where $\mathcal{S}_{L,t,i}$ is a slack variable. Constraints (PI-38) for *Operating Points 2* and 3 can be reformulated similarly.

C. Approximation of Confidence Bounds

The nonlinear, convex constraints (17), (28), and (29) include empirically-computed confidence bounds z_1 and z_2. We approximate these bounds with analytic functions and compare the performance and computational requirements of the approximations in Section IV.

1) Polyhedral Approximation: The polyhedral approximation introduces only linear inequalities, i.e.,

$$z(d) \ge \alpha_j d + \beta_j \,\forall\, j, \tag{39}$$

where α_j and β_j are parameters corresponding to linearization j.

2) 2-Norm Approximation: If M, in (15), were normally distributed with mean μ_M and standard deviation δ_M, and Y (which is normally distributed) has mean 0 and standard deviation δ_Y, then

$$z(d) = \mu_M + c\sqrt{(\delta_M)^2 + (d\delta_Y)^2}. \tag{40}$$

Since M is close to normally distributed at low violation levels, we can approximate it as such and compute μ_M and δ_M via nonlinear regression on the empirically-computed confidence bounds. Then each constraint including a confidence bound can be written as a linear constraint and a nonlinear slack variable constraint, where the latter is an SOC constraint. This approximation requires less memory than the polyhedral approximation.

TABLE I
COST DISTRIBUTION AND RESERVE ALLOCATION, $1-\varepsilon = 90\%$

		Scenario 1	Scenario 2	Analytical 1 & 2
Cost	Total	17320	17359	12778
	Dispatch	11941	11942	11867
	GS	904	950	0
	LS	237	232	56
	GD	4238	4235	855
Capacity (MW)	GS	181	190	0
	LS	474	464	112
	GD	2907	2905	855

TABLE II
COST DISTRIBUTION AND RESERVE ALLOCATION, $1-\varepsilon = 99\%$

		Scenario 1	Scenario 2	Analytical 1 & 2
Cost	Total	19657	19721	13474
	Dispatch	11978	11978	11876
	GS	2863	2938	0
	LS	97	90	87
	GD	4719	4716	1510
Capacity (MW)	GS	572	588	0
	LS	194	179	175
	GD	3162	3158	1370

D. Cutting Plane Algorithm

We use the cutting plane algorithm from [2] to reduce the computational effort associated with the SOC constraints, i.e., all of the slack variable constraints. In the first step of the algorithm, the CC-OPF is solved without the slack variable constraints. Then, all of the slack variable constraints are evaluated. If all are satisfied, we have obtained the solution to the full problem. Otherwise, we introduce linear constraints corresponding to first order Taylor series expansions of the unsatisfied slack variable constraints, re-solve the problem, check the slack variable constraints, and repeat until all are satisfied.

IV. CASE STUDIES

A. Set-Up

We use the same set-up as Part I. All results are generated using temperature forecast profile 5 (i.e., T case #5) and four intra-hour redispatch intervals, i.e., $n = 4$.

We compute and compare solutions for four test cases that differ in formulation and solution approach.

- *Scenario 1:* the formulation/approach used in Part I, i.e., the original constraints and original load capacities/baseline (see Fig. 1 of Part I), solved with the scenario-based method.
- *Scenario 2:* the approximate constraint (18) and the approximate load capacities/baseline in Fig. 1, solved with the scenario-based method.
- *Analytical 1:* the approximate constraint (18) and the approximate load capacities/baseline in Fig. 1, analytically reformulated using the *polyhedral approximation* of the confidence bounds and solved with i) a nonlinear solver and ii) the cutting plane algorithm.
- *Analytical 2:* the approximate constraint (18) and the approximate load capacities/baseline in Fig. 1, analytically reformulated using the *2-norm approximation* of the

TABLE III
COMPUTATIONAL TIME (S), NL = NONLINEAR SOLVER, CPA = CUTTING PLANE ALGORITHM

$1-\varepsilon$	Scenario 1	Scenario 2	Analytical 1 (NL)	Analytical 2 (NL)	Analytical 1 (CPA)	Analytical 2 (CPA)
90%	86.5	86.5	312.5	440.9	39.2	38.4
99%	76.1	77.7	314.4	433.2	38.9	38.8

confidence bounds and solved with i) a nonlinear solver and ii) the cutting plane algorithm.

We use the same uncertainty scenarios used in Part I. Specifically, for each test case, we conduct five simulation runs. The first set of runs corresponding to $1-\varepsilon = 90\%$ use the same 447 scenarios as used in Part I to compute the solutions for Scenario 1 and 2 and to compute the mean and covariance of the random variables for Analytical 1 and 2, and the same 10,000 scenarios as used in Part I to compute the empirical reliability, which is defined as one minus the empirical violation probability. The other four sets of runs corresponding to $1-\varepsilon = 90\%$ and five sets of runs corresponding to $1-\varepsilon = 99\%$ use different random selections of the uncertainty scenarios, where the same scenarios are used to both compute the solutions for Scenario 1 and 2 and to compute the mean and covariance of the random variables for Analytical 1 and 2. Therefore, the number of scenarios used to compute the mean and covariance of the random variables for Analytical 1 and 2 is different for $1-\varepsilon = 90\%$ and $1-\varepsilon = 99\%$.

B. Results

Tables I and II show the cost distribution and reserve allocation for the four test cases for $1-\varepsilon = 90\%$ and 99%, respectively, and for the first simulation run. The solutions corresponding to Scenarios 1 and 2 are more costly than those corresponding to Analytical 1 and 2, because the scenario-based method is more conservative since it uses extreme uncertainty scenarios from a probabilistically robust set. Subsequently, the scenario-based method procures more reserves leading to higher reserve costs and achieves less load shifting leading to higher dispatch costs. Additionally, we find that the solution corresponding to Scenario 2 is more costly/conservative than that corresponding to Scenario 1 since Scenario 2 uses the approximate load capacities and baseline. The approximation error results in small suboptimal changes to $P_{C,t}$ that reduce the ability of the loads to provide secondary reserves. The different approximations and solvers used in Analytical 1 and 2 do not affect the solutions or costs. Lastly, we find that decreasing ε increases reserve procurement and costs for all test cases. In Scenario 1 and 2, decreasing ε increases the number of uncertainty scenarios needed to generate the probabilistically robust set and, in Analytical 1 and 2, it increases $c = \Phi_N^{-1}(1-\varepsilon)$. Both changes tighten the feasible region.

Table III shows the computational time for the four test cases, for $1-\varepsilon = 90\%$ and 99%, where Analytical 1 and 2 are solved with both the nonlinear solver (NL) and the cutting plane algorithm (CPA). Results for all test cases correspond to the average of the five simulation runs. Table IV shows the breakdown of the computational time associated with solving Analytical 1 and 2 using the cutting plane algorithm. In each step, an optimization problem is solved and more constraints are added as the step increases from 1 to 4. For our problem, the algorithm converges after 4 steps. The column "Set-up" lists the total time between all iterations, which is required to compute the cuts.

While the computational times associated with Scenario 1 and 2 are smaller than those associated with Analytical 1 and 2 using the nonlinear solver, the computational times associated with Analytical 1 and 2 using the cutting plane algorithm are the smallest. Comparing our results to those of [7], we find that this computational advantage increases with problem dimension. The computational time of the first step of Analytical 2 is less than that of Analytical 1, but at Step 4 the computational time of Analytical 1 is less than that of Analytical 2. This is because Analytical 2 uses the 2-norm approximation, which includes a nonlinear slack variable constraint. New linear approximations of the constraint may be introduced in each step.

TABLE IV
BREAKDOWN OF THE COMPUTATIONAL TIME (S) USING THE CPA

	$1-\varepsilon$	Step 1	Step 2	Step 3	Step 4	Set-up
Analytical 1	90%	2.9	9.0	11.1	13.1	3.2
Analytical 1	99%	2.9	8.8	10.9	13.0	3.3
Analytical 2	90%	2.0	8.8	11.1	13.3	3.2
Analytical 2	99%	1.9	8.8	11.5	13.4	3.2

TABLE V
AVERAGE EMPIRICAL JOINT AND INDIVIDUAL RELIABILITY (%)

	$1-\varepsilon$	Scenario 1	Scenario 2	Analytical 1 & 2
Joint	90%	99.66	99.67	80.42
Individual	90%	100.00	100.00	99.54
Joint	99%	99.98	99.98	95.47
Individual	99%	100.00	100.00	99.89

TABLE VI
MAXIMUM AND MINIMUM EMPIRICAL JOINT RELIABILITY (%)

	$1-\varepsilon$	Scenario 1	Scenario 2	Analytical 1 & 2
Max	90%	100.00	100.00	88.77
Min	90%	98.15	98.49	75.51
Max	99%	100.00	100.00	97.42
Min	99%	99.87	99.87	94.38

TABLE VII
EMPIRICAL JOINT RELIABILITY BY CONSTRAINT TYPE FOR ANALYTICAL 1 & 2 (%)

	$1-\varepsilon = 90\%$	$1-\varepsilon = 99\%$
Power Flow	99.56	99.88
Energy Capacity	95.53	99.17
Operating Point 1	85.49	96.71
Operating Point 2	90.94	98.17
Operating Point 3	92.48	98.53

TABLE VIII
NUMBER OF CONSTRAINTS PER HOUR REQUIRED FOR THE SCENARIO-BASED METHOD

	Total	Linear	SOC
Deterministic, Equality	$6+N_C$	$6+N_C$	0
Deterministic, Inequality	$2N_L+11N_G+9N_C$	$2N_L+11N_G+9N_C$	0
Power Flow	$6N_L$	$6N_L$	0
Energy Capacity	$4N_C$	$4N_C$	0
Operating Point 1	$6N_G+4N_C$	$6N_G+4N_C$	0
Operating Point 2	$4N_G+2N_C$	$4N_G+2N_C$	0
Operating Point 3	$4N_G+2N_C$	$4N_G+2N_C$	0
Total	$6+25N_G+22N_C+8N_L$	$6+25N_G+22N_C+8N_L$	0

TABLE IX
NUMBER AND TYPE OF CONSTRAINTS PER HOUR REQUIRED FOR ANALYTICAL 1 AND 2

	Analytical 1 Linear	Analytical 1 SOC	Analytical 2 Linear	Analytical 2 SOC
Deterministic, Equality	$6+N_C$	0	$6+N_C$	0
Deterministic, Inequality	$2N_L+11N_G+9N_C$	0	$2N_L+11N_G+9N_C$	0
Power Flow	0	$6N_L$	0	$6N_L$
Energy Capacity	$2jN_C$	$2N_C$	0	$4N_C$
Operating Point 1	$4N_G+(2+j)N_C$	$2N_G+N_C$	$4N_G+2N_C$	$2N_G+2N_C$
Operating Point 2	jN_C	$4N_G+N_C$	0	$4N_G+2N_C$
Operating Point 3	0	$4N_G+(1+j)N_C$	0	$4N_G+2N_C$
Total	$6+15N_G+(12+4j)N_C+2N_L$	$10N_G+(5+j)N_C+6N_L$	$6+15N_G+12N_C+2N_L$	$10N_G+10N_C+6N_L$

Table V shows the average empirical joint and individual reliability of the solutions associated with each of the test cases, where the average is taken over the five simulation runs. Table VI shows the maximum and minimum empirical joint reliability across the five simulation runs.[1] The joint reliability is the percent of hourly sets of constraints that are satisfied concurrently considering all of the scenarios, whereas the individual reliability is the percent of constraints that are satisfied individually considering all scenarios. Recall that the scenario-based method satisfies constraints jointly, while the analytical reformulation is only capable of satisfying constraints individually.

As shown in Table V, Scenario 1 and 2 are conservative, achieving empirical joint reliabilities well-above the desired joint reliability. Analytical 1 and 2 achieve much lower empirical joint reliabilities, but do achieve empirical individual reliabilities well-above the desired individual reliability because, for each uncertainty scenario, few constraints are active. Increasing $1-\varepsilon$ from 90% to 99% improves the empirical joint reliability of Analytical 1 and 2 indicating that c could be tuned to achieve the desired joint reliability. As shown in Table VI, the empirical joint reliability of Analytical 1 and 2 varies more than that of Scenario 1 and 2, but increasing $1-\varepsilon$ decreases the range.

Table VII shows the empirical joint reliability by constraint type for Analytical 1 and 2. The first row (Power Flow) corresponds to all of the power flow constraints for all three operating points; the second row (Energy Capacity) corresponds to all controllable load energy capacity constraints; the third row (Operating Point 1) corresponds to all generation, controllable load power capacity, and reserve capacity constraints corresponding to *Operating Point 1*; the fourth row (Operating Point 2) corresponds to all generation, controllable load power capacity, and reserve capacity constraints corresponding to *Operating Point 2*; and the fifth row (Operating Point 3) corresponds to all generation, controllable load power capacity, and reserve capacity constraints corresponding to *Operating Point 3*, except the redundant constraints included in Operating Point 1. Power flow and energy capacity constraints have high joint reliability because they are rarely active. In contrast, reserve capacity constraints, which are included within the operating point constraints, are generally active since we attempt to minimize reserve capacities while providing enough reserves to compensate for wind power and temperature forecast error. This point is also demonstrated by the large improvement in the joint reliability of Operating Point 1–3 constraints as we increase $1-\varepsilon$ from 90% to 99%.

To summarize how the solution approaches scale, Tables VIII and IX show the number of constraints per hour required by the scenario-based method and the analytical reformulations, respectively. We split the constraints by type and by form, i.e., linear v.s. SOC constraints. As before, N_W is the number of wind power plants, N_T is the number of temperature zones, N_C is the number of controllable load aggregations, and j is the number of linear inequalities introduced by the polyhedral approximation in Analytical 1. We also define N_G as the number of conventional generators and N_L as the number of transmission lines. The number of decision variables per hour is $10N_G+4N_C$. Observe that N_W and N_T do not affect the number of constraints, but do affect the size of the matrices/vectors used to represent the constraints. These tables can be used to determine the increased computational effort required for increased system sizes and to determine the composition of constraints for Analytical 1 and 2. Commercial solvers normally use primal-dual interior point methods to solve optimization problems. Complexity bounds for SOC programs are given in [8] and for quadratic programs are given in [9] and [10].

[1]The minimum empirical joint reliability for Scenario 1, $1-\varepsilon=90\%$, i.e., 98.15%, is comparable to the worse-case hourly empirical violation probability reported in Part I, i.e., 1.86%.

V. Conclusion

In this paper, we analytically reformulated the chance-constrained optimal power flow problem with uncertain controllable loads assuming temperature and wind power forecast uncertainty follow multivariate normal distributions. We showed that the nonlinear formulation is convex and we demonstrated how to compute empirical confidence bounds for the nonlinear constraints. We also showed how to approximate the confidence bounds with two different convex approximations and use an iterative cutting plane algorithm to reduce computational times. Through simulations, we compared the costs, solutions, computational times, and reliability of the approach to that of the scenario-based method introduced in Part I. We showed that the analytical reformulation provides less conservative, lower cost solutions with empirical individual reliabilities above desired individual reliabilities. However, the approach does not guaranteed joint chance-constraint satisfaction and so empirical joint reliabilities are much lower than that of the scenario-based method. Still, joint reliabilities can be increased by heuristically tuning the desired individual reliability. Importantly, the analytical reformulation solved with the cutting plane algorithms requires less computational time than the scenario-based method for the test system used, and we provided tables demonstrating the scalability of the approaches as a function of the problem size.

Future research will include i) improving the models and ii) exploring the benefits of the wide variety of emerging stochastic optimization techniques in development for CC-OPF problems. For the former, we will attempt to model the AC power flows, leveraging recent results, e.g., [11] and [12]. For the latter, we will explore alternative robust optimization techniques that have been applied to related CC-OPF problems, e.g., [13]–[15], including distributionally robust optimization, e.g., [4], [16], and [17].

Appendix A
Confidence Bound Derivation

In this Appendix, we derive the confidence bound $z_1(d_{LS,t})$ corresponding to one of the N_C constraints in (17) for Case 1 (i.e., $T_t^f < T_{br}$) at one time interval t. Other confidence bounds can be derived similarly.

Without loss of generality, assume the mean of $X = \Delta T_t \in \mathbb{R}$ is 0 and the standard deviation is δ_X. Then, the probability density function (PDF) of X is

$$f_X(x) = \frac{1}{\delta_X\sqrt{2\pi}}\exp\left(-\frac{x^2}{2\delta_X^2}\right), \tag{41}$$

and the CDF of M, defined in (15), is

$$\mathbb{P}(M \le m) = F_X\left(\frac{m-h}{k_2}\right) - F_X\left(\frac{m}{k_1}\right), \tag{42}$$

where F_X is the CDF of X, $k_1 = a$, $k_2 = a - k_p$, and $h = k_p e_{T,t}$. The PDF of M is

$$\begin{aligned} f_M(m) = \frac{d\mathbb{P}(M \le m)}{dm} &= \frac{f_X\left(\frac{m-h}{k_2}\right)}{k_2} - \frac{f_X\left(\frac{m}{k_1}\right)}{k_1} \\ &= \frac{f_X\left(\frac{m-h}{k_2}\right)}{k_2} + \frac{f_X\left(\frac{m}{-k_1}\right)}{-k_1} \end{aligned} \tag{43}$$

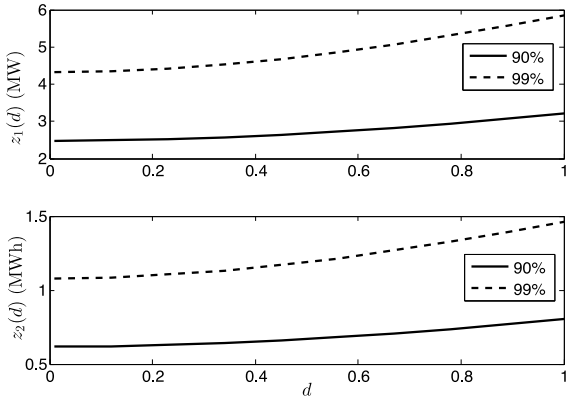

Fig. 2. Example confidence bounds $z_1(d)$ and $z_2(d)$ for $1-\varepsilon = 90\%$ and $1-\varepsilon = 99\%$.

since f_X is symmetric with respect to zero.

Similarly, assume the mean of $dY = d_{LS,t}P_{m,t} \in \mathbb{R}$ is 0 and the standard deviation is $d\delta_Y = d_{LS,t}\overline{\delta}_{W,t}$. The PDF of dY is

$$f_{dY}(y) = \frac{1}{d\delta_Y\sqrt{2\pi}}\exp\left(-\frac{y^2}{2(d\delta_Y)^2}\right) \tag{44}$$

Since $h < 0$, $k_1 < 0$, and $k_2 > 0$, M is lower bounded by some value $-C_3 < 0$. Therefore, the CDF of Z is

$$\begin{aligned} \mathbb{P}(Z \le z_1(d)) &= \int_{-C_3}^{\infty}\int_{-\infty}^{z_1(d)-m} f_M(m) f_{dY}(y)\,\mathrm{d}y\,\mathrm{d}m \\ &= \int_{-C_3}^{\infty} f_M(m)\,\Phi_N\left(\frac{z_1(d)-m}{d\delta_Y}\right)\mathrm{d}m. \end{aligned} \tag{45}$$

We solve for $z_1(d)$ empirically by setting (45) equal to $1-\varepsilon$ and sweeping discrete values of d within its domain, i.e., [0, 1]. Examples of the confidence bounds are shown in Fig. 2.

Appendix B
Monotonicity and Convexity Proof Sketches

All constraints with the exception of those that include confidence bounds are clearly convex. Figure 2 shows that the empirically-computed confidence bounds appear to be convex. In this Appendix, we sketch the proofs of monotonicity and convexity for the confidence bound considered in Appendix A. Similar reasoning can be used to prove monotonicity and convexity for all other confidence bounds, and so all constraints within this paper that include confidence bounds are convex.

Assuming we have a solution triple (d_0, z_0, P_0) corresponding to $(d_{LS,t}, z_1(d_{LS,t}), 1-\varepsilon)$ and we pick a large P_0 such that $z_0 > C_3$ and the integral in (45) corresponding to $m \in [2z_0 + C_3, \infty]$ is negligible (because this region corresponds to the tail of f_M), we have

$$\mathbb{P}(Z \le z_0) = \int_{-C_3}^{2z_0+C_3} f_M(m)\,\Phi_N\left(\frac{z_0-m}{d_0\delta_Y}\right)\mathrm{d}m = P_0, \tag{46}$$

$$\min_{m\in[-C_3,z_0]} f_M(m) = f_M(z_0), \tag{47}$$

$$\max_{m\in[z_0,\infty]} f_M(m) = f_M(z_0). \tag{48}$$

Increasing d_0 to d_1, the change in P_0 is

$$\int_{-C_3}^{2z_0+C_3} f_M(m) \underbrace{\left[\Phi_N\left(\frac{z_0-m}{d_1\delta_Y}\right)-\Phi_N\left(\frac{z_0-m}{d_0\delta_Y}\right)\right]}_{\Delta\Phi} \mathrm{d}m$$
$$= \int_{-C_3}^{z_0} (f_M(m) - f_M(2z_0-m))\Delta\Phi \,\mathrm{d}m, \tag{49}$$

since Φ_N is symmetric with respect to z_0. From (47) and (48) we know that $f_M(m) - f_M(2z_0 - m) \geq 0 \in [-C_3, z_0]$. We also know that $\Delta\Phi < 0 \in [-C_3, z_0]$. Hence, the change in P_0 is negative and to increase P_0 we would need to increase z_0. Therefore, for a fixed P_0, which is above some threshold ensuring that the above assumptions hold, $z(d)$ will monotonically increase.

Proving convexity also requires approximations on the tails of the PDFs. Though f_M is the summation of two normal PDFs, as shown in (43), one tail will dominate the other for large P_0. Hence, when we increase d_0 to d_1 the change in P_0 will be approximately the same as the change that would occur if f_M corresponded to a single normal PDF. Therefore, for a fixed P_0, which is above some threshold ensuring that the above assumptions hold, $z(d)$ will be convex and, when d is a scalar, the corresponding constraint will be convex. When d is a vector, constraint convexity requires $z(d)$ be monotonic, which was shown above. This conclusion is supported by our simulation results, which demonstrate that 2-norm approximations of the confidence bounds are accurate for large P_0.

REFERENCES

[1] K. Margellos, P. Goulart, and J. Lygeros, "On the road between robust optimization and the scenario approach for chance constrained optimization problems," *IEEE Trans. Autom. Control*, vol. 59, no. 8, pp. 2258–2263, Aug. 2014.

[2] D. Bienstock, M. Chertkov, and S. Harnett, "Chance-constrained optimal power flow: Risk-aware network control under uncertainty," *SIAM Rev.*, vol. 56, no. 3, pp. 461–495, 2014.

[3] L. Roald, F. Oldewurtel, T. Krause, and G. Andersson, "Analytical reformulation of security constrained optimal power flow with probabilistic constraints," in *Proc. IEEE PowerTech*, Grenoble, France, Jun. 2013, pp. 1–6.

[4] Y. Zhang, S. Shen, and J. L. Mathieu, "Distributionally robust chance-constrained optimal power flow with uncertain renewables and uncertain reserves provided by loads," *IEEE Trans. Power Syst.*, vol. 32, no. 2, pp. 1378–1388, Mar. 2017.

[5] S. P. Boyd and L. Vandenberghe, *Convex Optimization*. Cambridge, U.K.: Cambridge Univ. Press, 2004.

[6] M. Lubin, D. Bienstock, and J. P. Vielma, "Two-sided linear chance constraints and extensions," *arXiv preprint arXiv:1507.01995*, 2015. [Online]. Available: https://arxiv.org/abs/1507.01995

[7] B. Li and J. L. Mathieu, "Analytical reformulation of chance-constrained optimal power flow with uncertain load control," in *Proc. IEEE PowerTech*, Eindhoven, The Netherlands, Jun. 2015, pp. 1–6.

[8] Y. Q. Bai and G. Q. Wang, "Primal-dual interior-point algorithms for second-order cone optimization based on a new parametric Kernel function," *Acta Math. Sinica*, vol. 23, no. 11, pp. 2027–2042, 2007.

[9] G.-Q. Wang, Y.-Q. Bai, Y. Liu, and M. Zhang, "A new primal-dual interior-point algorithm for convex quadratic optimization," *J. Shanghai Univ. (English Ed.)*, vol. 12, no. 3, pp. 189–196, 2008.

[10] X. Cai, G. Wang, and Z. Zhang, "Complexity analysis and numerical implementation of primal-dual interior-point methods for convex quadratic optimization based on a finite barrier," *Numer. Algorithms*, vol. 62, no. 2, pp. 289–306, 2013.

[11] M. Vrakopoulou, M. Katsampani, K. Margellos, J. Lygeros, and G. Andersson, "Probabilistic security-constrained AC optimal power flow," in *Proc. IEEE PowerTech*, Grenoble, France, 2013, pp. 1–6.

[12] E. Dall'Anese, K. Baker, and T. Summers, "Chance-constrained AC optimal power flow for distribution systems with renewables," *IEEE Trans. Power Syst.*, vol. 32, no. 5, pp. 3427–3438, Sep. 2017.

[13] R. A. Jabr, "Adjustable robust OPF with renewable energy sources," *IEEE Trans. Power Syst.*, vol. 28, no. 4, pp. 4742–4751, Nov. 2013.

[14] R. A. Jabr, S. Karaki, and J. A. Korbane, "Robust multi-period OPF with storage and renewables," *IEEE Trans. Power Syst.*, vol. 30, no. 5, pp. 2790–2799, Sep. 2015.

[15] M. Lubin, Y. Dvorkin, and S. Backhaus, "A robust approach to chance constrained optimal power flow with renewable generation," *IEEE Trans. Power Syst.*, vol. 31, no. 5, pp. 3840–3849, Sep. 2016.

[16] T. Summers, J. Warrington, M. Morari, and J. Lygeros, "Stochastic optimal power flow based on conditional value at risk and distributional robustness," *Int. J. Elect. Power Energy Syst.*, vol. 72, pp. 116–125, Nov. 2015.

[17] L. Roald, F. Oldewurtel, B. Van Parys, and G. Andersson, "Security constrained optimal power flow with distributionally robust chance constraints," *arXiv preprint arXiv:1508.06061*, 2015. [Online]. Available: https://arxiv.org/abs/1508.06061

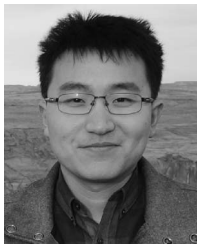

Bowen Li (S'12) received the B.S. degree in mechanical engineering from Shanghai Jiao Tong University, Shanghai, China, and the B.S. and M.S. degrees in electrical engineering from the University of Michigan, Ann Arbor, MI, USA, in 2013 and 2015, respectively, where he is currently pursuing the Ph.D. degree in electrical engineering. His research interests include developing and evaluating models and formulations used in stochastic optimal power flow problems with uncertainties from renewable resources and demand response.

Maria Vrakopoulou (S'09–M'14) received the Diploma degree in electrical and computer engineering from the University of Patras, Greece, in 2008, and the Ph.D. degree from the Department of Electrical Engineering and Information Technology, ETH Zurich, Switzerland, in 2013. She pursued her research as a Post-Doctoral Fellow with the University of Michigan, Ann Arbor, MI, USA, and the University of California at Berkeley, Berkeley, CA, USA. Since 2017, she has been a Marie Curie Post-Doctoral Fellow with the Automatic Control Laboratory, Department of Electrical Engineering and Information Technology, ETH Zurich. Her research interest concentrate on the optimization and analysis of planning problems for power systems under uncertainty.

Johanna L. Mathieu (S'10–M'12) received the B.S. degree in ocean engineering from the Massachusetts Institute of Technology, Cambridge, MA, USA, in 2004 and the M.S. and Ph.D. degrees in mechanical engineering from the University of California at Berkeley, Berkeley, USA, in 2008 and 2012, respectively. She was a Post-Doctoral Researcher with the Swiss Federal Institute of Technology (ETH) Zurich, Switzerland. She is an Assistant Professor with the Department of Electrical Engineering and Computer Science, University of Michigan, Ann Arbor, MI, USA. Her research interests include modeling, estimation, control, and optimization of distributed energy resources.